Modern Environmental Science and Engineering (ISSN 2333-2581)
April 2024, Volume 10, No. 3-4, pp. 39-46
Doi: 10.15341/mese(2333-2581)/3-4.10.2024/001
Academic Star Publishing Company, 2024
www.academicstar.us

Deformation Detection in the Socompa Volcano (Province of Salta, Argentina) Using Radar Interferometric Method (SBAS)

Eugenia Mariana Wright, María Laura Pardo Duró, and Federico Carballo
Argentina Geological Mining Survey and University of Buenos Aires, Argentina

Abstract: The remote sensing area of the Geomatics Department of SEGEMAR (Argentina Geological Mining Survey) monitors the 39 volcanoes considered active in the Argentine Republic. Each volcano is analyzed by SAR (Synthetic Aperture Radar) image processing applying InSAR (SAR Interferometry) techniques to identify deformation. In July 2021, an anomalous pattern was observed at the Socompa volcano. Consequently, a more detailed analysis was carried out by generating 2 time series of Sentinel-1 images with DInSAR SBAS (Differential SAR Interferometry Small BAseline Subset) technique in order to analyze its spatio-temporal characteristics. The Socompa volcano (24.3963°S 68.2456°W) is an active volcano of Quaternary age located in the Province of Salta, on the border between Argentina and Chile. The presence of fumaroles near its crater and other thermal manifestations such as springs that outcrop on the shore of saline lagoons, hot springs at the base of the volcanic edifice and the presence of warm soils suggest the existence of an anomalous thermal gradient in the region. The strong evidence of hydrothermal activity under the volcanic edifice is probably associated with the magmatic chamber that is still active inside it. This work shows the results obtained for ascending and descending time series of SAR images for the period October 2014–July 2023, evidencing deformation of the volcano.

Key words: Socompa Volcano, DInSAR SBAS, deformation, time series

1. Introduction

The remote sensing area of the Geomatics Department of SEGEMAR (Argentina Geological Mining Survey) monitors the 39 volcanoes considered active in the Argentina Republic. In order to analyze the evolution of deformation in volcanoes at different time periods, DInSAR technique is applied to Sentinel-1 Synthetic Aperture Radar (SAR) images.

SAR Interferometry is used to detect surface deformation that may be associated with various phenomena such as volcanic activity and seismic events [1-5]. It relies on the phase information available in SAR signal to measure the path difference between two acquisitions made at different times and their orbital positions. The result is a relief map of the change in distance between the surface and the radar [6], and movements in the topography can be recorded with centimetric accuracy.

In the analysis performed at Socompa volcano in July 2021, an anomalous pattern compatible with deformation was evidenced on the slopes of the volcanic edifice. This pattern was repeated when applying the same technique with different interferometric pairs in order to rule out an atmospheric effect that could be influencing the result. Consequently, a more detailed analysis with time series derived from SAR image processing, both ascending and descending paths was performed. The generation of time series and average velocity maps is an effective way to study the dynamics of deformation phenomena and their temporal behaviour. This is possible by

Corresponding author: Eugenia Mariana Wright, Doctor; research areas/interests: remote sensing, SAR, surface deformation, DInSAR, time series. E-mail: eugenia.wright@segemar.gov.ar.

combining information obtained from multiple SAR images over a given period of time.

Background information on deformation analysis at Socompa volcano was first cited by Wright *et al.* [7] and afterwards by Liu *et al.* [8]. In October 2022, Wright *et al.* [7] analyzed the deformation from ascending and descending Sentinel-1 time series between January 2018 and May 2022 and identified an uplifting from mid-2020 onwards with a displacement velocity of approximately 1 cm/year and a cumulative displacement of ~5 cm over the entire period. Subsequently, Liu Feng *et al.* [8] measured the same deformation between January 2018 and October 2021 with InSAR and GPS observations from the Nevada Geodetic Laboratory and identified a steady uplift up to 17.5 mm/year from December 2019 to the end of the studied period. Other studies on Socompa volcano analyze its magmatic chamber as well as its geothermal reservoir. The presence of a magmatic chamber in the Socompa volcano area, located between 2 and 7 km depth, was determined by deep geophysical prospecting using the long-period magnetotelluric (MT) technique [9]. This chamber constitutes the heat source that feeds the thermal manifestations located in the area of the Socompa lagoon and explains the presence of hot vaporous fumarolic soils in the crater of the volcano. The permanent geothermal fluid circulation and the presence of a shallow reservoir with high probability of containing thermal brine, occurs in a structural setting that favours the distribution and storage of hot fluids [10].

The aim of this work is to analyze the deformation pattern observed in the interferograms of the Socompa volcano with Radar Interferometric SBAS time series.

2. Material and Methods

2.1 Methods

2.1.1 Study Area

Socompa Volcano and surrounding area, approximately 30 km radius, will be the focus of study. Socompa volcano (24.3963° S - 68.2456° W) is a Quaternary volcano, located in the Province of Salta, on the border between Argentina and Chile (Fig. 1).

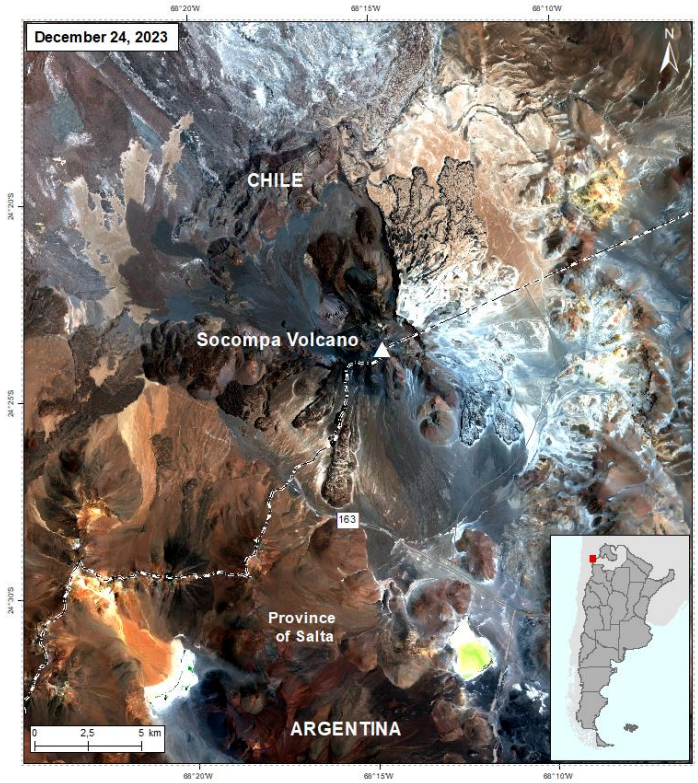

Fig. 1 Location of Socompa Volcano in a Sentinel 2 Image RGB 432 of December 24, 2023.

The growth of the Socompa volcano includes lava flows, domes and minor fall deposits [11] and a remarkable collapse of the main body of the volcano that produced a debris flow of 25 km^3 7,200 years ago. The post-collapse lava flows, of which only a minor part outcrops in Argentine territory cover the flow deposit, making this its maximum age [11, 12]. These allows Socompa to be included in the category of active volcano, the most evident indication of which is the existence of fumarolic activity in the vicinity of its crater [11].

The presence of fumaroles near its crater and other thermal manifestations located in the Socompa lagoon and in the Quebrada del Agua, such as springs that outcrop on the shores of saline lagoons, thermal waters at the base of the volcanic edifice and the presence of warm soils, suggest the existence of an anomalous thermal gradient in the region. Strong evidence of hydrothermal activity beneath the volcano is probably associated with the magma chamber that is still active within it [11, 13].

2.1.2 Data Used

The following data was used for the generation of sixteen phase interferograms with Sentinel-1 images:

• Sixteen Sentinel-1 SLC IW (Interferometric Wide) images from ascending path.

• Eleven Sentinel-1 SLC IW images from descending path.

Table 1 shows the time intervals of the sixteen Sentinel-1 interferometric pairs analyzed.

Data used for the generation of ascending and descending paths time series:

• 100 Sentinel-1 SLC IW of ascending path

• 98 Sentinel-1 SLC IW of descending path

Table 2 shows the time lapse of each time series, as well as the number of scenes used and the interferograms generated.

GNSS field data from the Nevada Geodetic Laboratory's SOCM Station (24.455°S, 68.295°W) [14] was also used to compare with the deformation observed with DInSAR.

Table 1 Interferometric pairs of Sentinel-1 images of Socompa volcano.

Interferometric pairs	Path
20170309 - 20210710	Ascending
20171005 - 20210511	Ascending
20180115 - 20211213	Ascending
20180602 - 20210704	Ascending
20180602 - 20210710	Ascending
20180620 - 20210628	Ascending
20190510 - 20210704	Ascending
20200814 - 20210920	Ascending
20180115 - 20231203	Ascending
20191118 - 20231109	Ascending
20180122 - 20211220	Descending
20190722 - 20210729	Descending
20200821 - 20210921	Descending
20180715 - 20230911	Descending
20180110 - 20231204	Descending
20191113 - 20231110	Descending

Table 2 Sentinel-1 scenes used for the ascending and descending time series of the Socompa volcano.

Time lapse	Path	N° Scenes	N° Interferograms
October 2014 – July 2023	Ascending	100	291
May 2015 – July 2023	Descending	98	460

2.2 DInSAR Methods

In a first stage, DInSAR technique was applied to identify surface deformation from interferometric pairs of SAR images acquired at different time intervals between 2017 and 2023. The ISCE software (InSAR Scientific Computing Environment) developed by Standford University, JPL and Caltech was used for this processing.

The second stage involved the analysis of time series performed with the DInSAR SBAS (Small BAseline Subset) technique, based on an appropriate combination of differential interferograms formed by pairs of data characterized by a small orbital separation (baseline) to limit spatial decorrelation phenomena [15]. This technique uses a huge amount of SAR data, providing maps of surface deformation over long

periods of time with sub-centimeter accuracy and making possible the analysis of slow surface motion deformation. The software used for this processing was MintPy (Miami INsar Time-series software in Python) in combination with the previously mentioned ISCE. MintPy is an open source package for the analysis of Interferometric Synthetic Aperture Radar (InSAR) time series.

The time series were generated from October 2014 to July 2023 for the ascending path and from May 2015 to July 2023 for the descending one. The difference between the time period covered by each series is due to the availability of scenes.

As tropospheric delays are the main source of error when measuring ground displacements using DInSAR [16], a tropospheric correction was applied. Python based Atmospheric Phase Screen estimation (PyAPS) correction uses data from ERA5 Global Atmospheric Model (GAM). It is a correction based on data from the European Centre for Medium-Range Weather Forecasts (ECMWF) 5th Generation Reanalysis (ERA5) [17].

3. Results and Discussion

3.1 DInSAR Results

Several phase interferograms were obtained at time intervals of between 1 and 6 years, for both ascending and descending paths, in order to rule out possible atmospheric influences or topography-associated effects. Those with time intervals greater than 3 years evidence a pattern associated with deformation showing a surface uplifting of approximately 2.8 cm and the ones with time intervals greater than 6 years, 5.6 cm between the analyzed dates. Interferograms in Fig. 2 illustrates the pattern observed between November 18, 2019 and November 9, 2023, in the ascending path, and between November 13, 2019 and November 10, 2023 in the descending one.

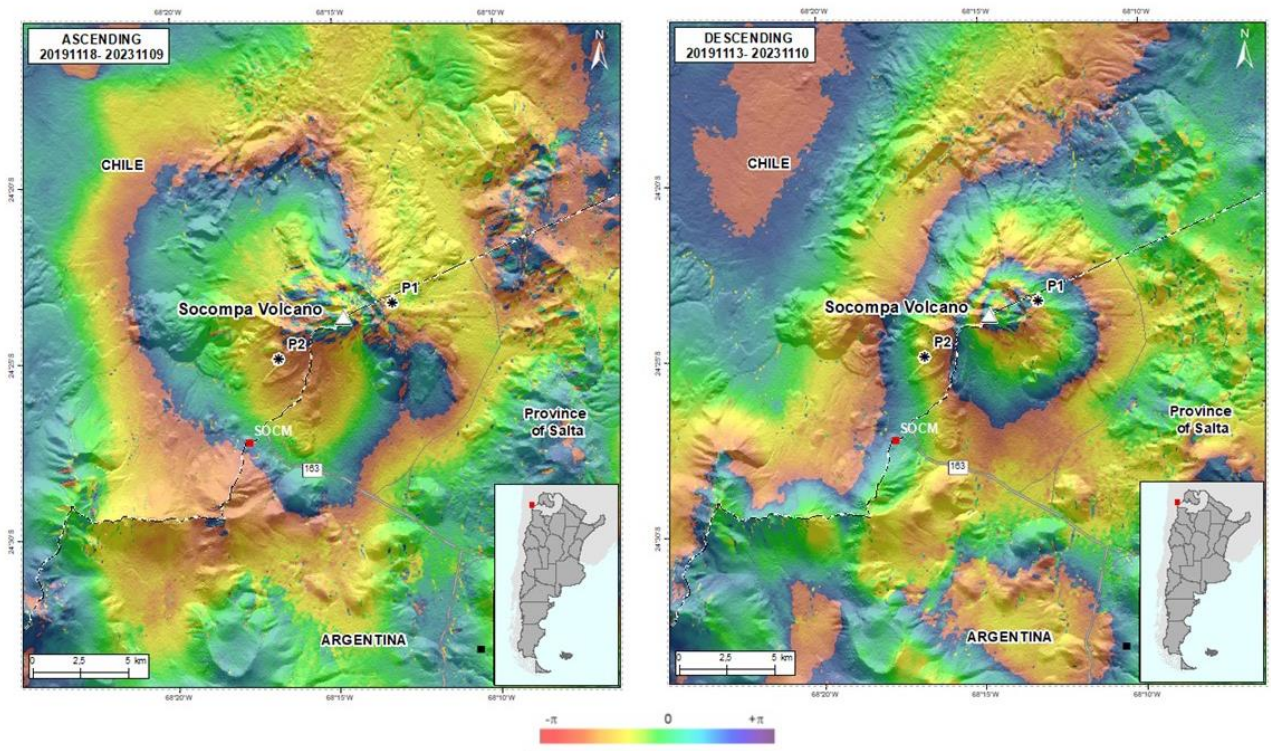

Fig. 2 Interferograms of Socompa volcano generated with Sentinel-1: Ascending path interferogram between November 18, 2019 and November 9, 2023 (on the left). Descending path interferogram between November 13, 2019 and November 10, 2023 (on the right).

Based on the results obtained from the interferometry processing, time series were generated with Sentinel-1 scenes to characterize and quantify the identified pattern.

3.2 DInSAR SBAS — Time Series Results

The result of both ascending and descending time series shows an uplifting pattern over the volcano (Fig. 3) with a mean velocity in the line of sight (LOS) direction of approximately 1 cm/year, coinciding with the displacement observed in the different interferograms previously generated.

Both series were calculated with respect to a high stability reference point located at 24.554°S, 68.176°W (black square in Fig. 3). The location of the deformation is found tilted towards the W slope in the ascending series and towards the E-SE slope in the descending series. This is due to the different angle of gaze depending on the orbit and it gives an indication of the predominant direction of displacement.

The displacement was calculated for two points located on opposite sides of the volcano, point 1 on the east slope (P1: 24.390°S, 68.219°W) and point 2 on the southwest slope (P2: 24.416°S, 68.279°W) (Fig. 2 and Fig. 3).

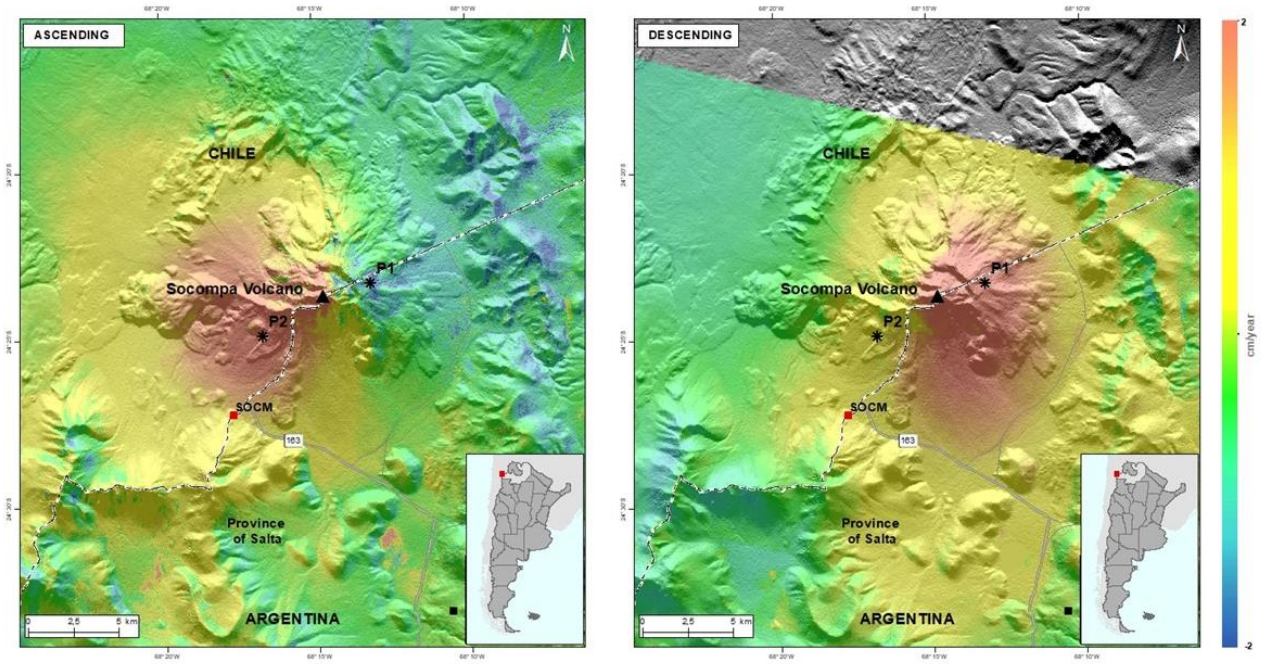

Fig. 3 Mean displacement velocity in the LOS (cm/year) of Socompa Volcano between October 27, 2014 and July 12, 2023 in the Ascending path time series (on the left) and between May 20, 2015 and July 13, 2023 in the Descending path time series (on the right).

The descending series at P1 and P2 (Fig. 4A and B) show a break of stability and the beginning of an inflationary process from mid-2020 onwards (dotted green line in both figures). P1 shows a total cumulative uplifting displacement of approximately 4 cm in the last 3 years (mid-2020 to mid-2023), with a mean LOS velocity of ~0.97 cm/year (Fig. 5), while P2 shows a less significant inflationary trend with a total cumulative uplifting displacement of approximately 1 cm in the same period. In the ascending series, an almost constant deflationary process is observed at P1 during the whole analyzed period, with a mean velocity in the LOS of -0.79 cm/year. This negative displacement of P1 indicates that the inflationary process is predominantly eastward. As for P2, the series is similar to that of the descending path, with no apparent displacement until mid-2020. From that moment, the total cumulative uplifting displacement is

approximately 5 cm in 3 years of analysis and the calculated mean displacement velocity in the LOS, of ~1.06 cm/year (Fig. 5).

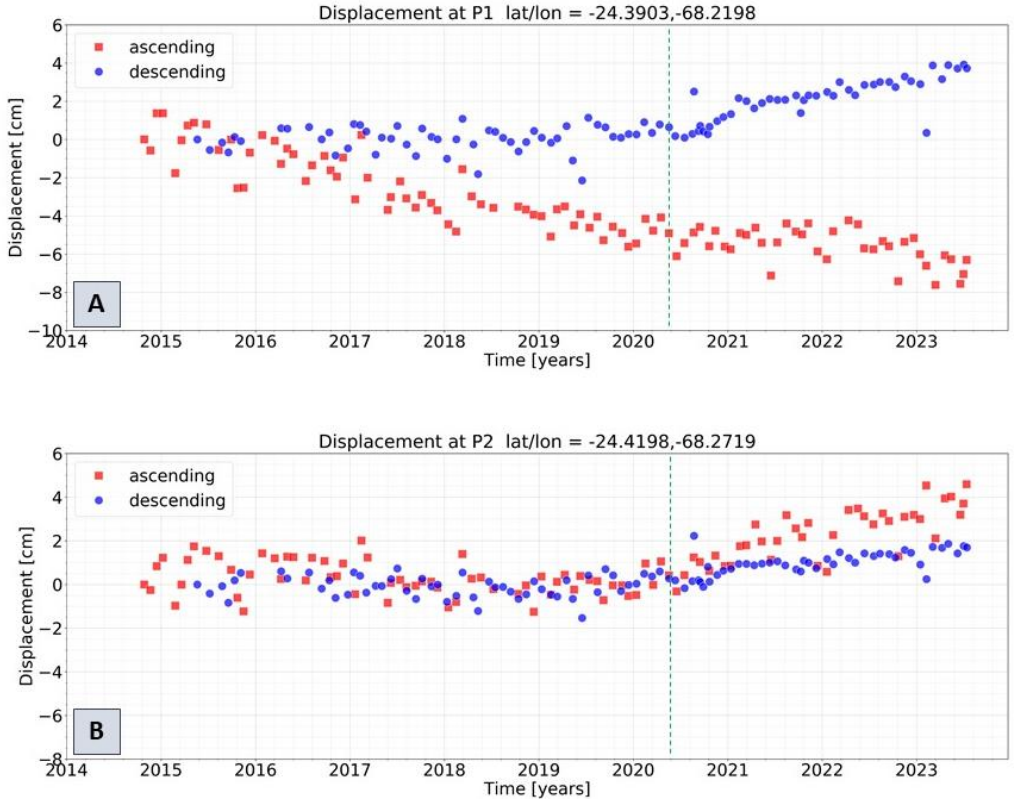

Fig. 4 Comparison of the cumulative displacement series on the sensor line of sight (LOS) for point 1 (A) located on the east slope of Socompa Volcano (24.390°S, 68.219°W) and point 2 located on the southwest slope (24.416°S, 68.279°W) in both paths, Ascending and Descending, between October 2014 and July 2023 and between May 2015 and July 2023, respectively.

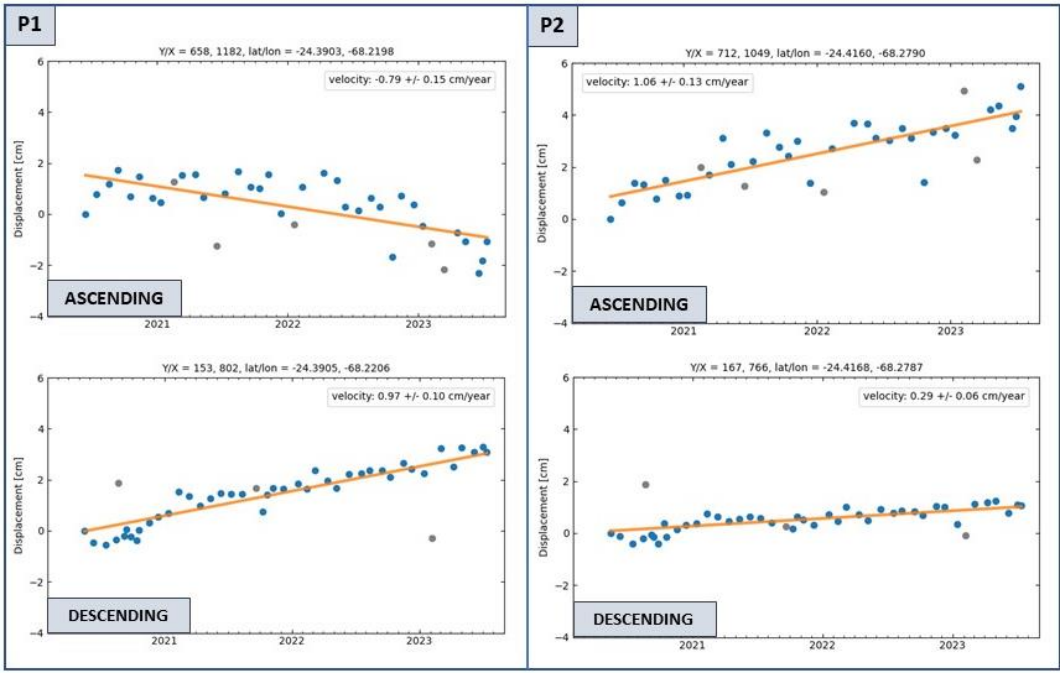

Fig. 5 Point Displacement Time series on the sensor line of sight (LOS) between July 2020 and July 2023. P1 in the ascending and descending paths (on the left) and P2 in the ascending and descending paths (on the right).

GNSS measurements from the SOCM Station from the Nevada Geodetic Laboratory [14] located at 24.455°S, 68.295°W (red square in Fig. 2 and Fig. 3) shows, in the vertical component, an uplift of 30 mm from mid-2020 to the beginning of 2023 (Fig. 6). P2 is the one located closest to the SCOM station.

3.3 Discussions

Both the ascending and descending time series show an inflationary process at Socompa volcano of approximately 1 cm/year from August 2020 to the end of the series.

P2 located on the southwestern slope of the volcano shows a lower displacement velocity in the descending series, which would indicate that the center of the uplifting process is located on the south slope of the volcano.

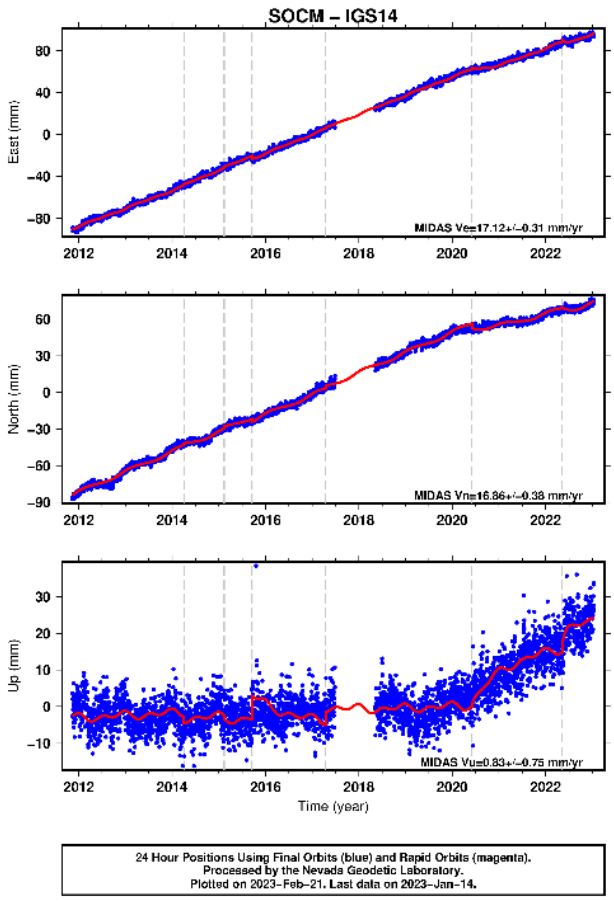

Fig. 6 GNSS Point offset - Station ID: SOCM Nevada Geodetic Laboratory [14].

P1 in the ascending path shows a constant negative displacement since the beginning of 2017, indicating a shift away from the sensor. The first signs of deformation could be identified in the P1. It should be noted that SCOM station data show a deformation starting shortly before the one identified with DINSAR.

The analysis of the deformation of the Socompa volcano requires further studies to define the causes of the uplifting process identified.

4. Conclusions

The time series analysis of Sentinel-1 images, using ISCE and MintPy software, allowed to quantify the displacement and calculate the mean velocity in LOS of the pattern observed in the interferograms of the Socompa volcano.

Two SAR time series were generated and in both of them an inflationary trend is observed from mid-2020 onwards, with an observed mean displacement velocity in the LOS of approximately 1 cm/year.

The total cumulative displacement from the beginning of the series, from 2014 to 2023, shows a rise of approximately 4 cm over the 9 years analyzed, and is mostly produced in the last 3 years, between August 2020 and July 2023.

The analysis of the spatial-temporal behaviour of 2 points located on the east and southwest slopes of the volcano shows that at point 1 the deformation would have an easterly orientation, approaching the sensor in the descending orbit and moving away in the ascending one. Point 2 shows an approach in both orbits, indicating that the inflationary process could have a south direction.

The extension of the SAR time series and further work is required to assess the origin of the uplifting process identified, as well as the precise direction of the displacement.

References

[1] Astort, A., Walter, T. R., Ruiz, F., Sagripanti, L., & Nacif,

A. A. (2019). Unrest at Domuyo Volcano, Argentina, detected by geophysical and geodetic data and morphometric analysis, Multidisciplinary Digital Publishing Institute, *Remote Sensing 11* (18): 1–28.

[2] Cigna, F., Osmanoğlu, B., Cabral-Cano, E., Dixon, T. H., Ávila-Olivera, J. A., Garduño Monroy, V. H., DeMets, C. & Wdowinski S. (2012). Monitoring land subsidence and its induced geological hazard with synthetic aperture radar interferometry: A case study in Morelia, Mexico, *Remote Sensing of Environment* 117: 146–161.

[3] Goldstein, R. M., & Werner, C. L. (1998). Radar interferogram filtering for geophysical applications, *Geophysical Research Letters 25* (21): 4035–4038.

[4] Lanari, R., Berardino, P., Bonano, M., Casu, F., Manconi, A., Manunta, M., Manzo, M., Pepe, A., Pepe, S., & Sansosti, E. (2010). Surface displacements associated with the l'aquila 2009 mw 6.3 earthquake (central italy): New evidence from SBAS-DInSAR time series analysis, *Geophysical Research Letters 37* (20).

[5] Velez, M. L., Euillades, P., Caselli, A., Blanco, M., & Díaz, J. M. (2011). Deformation of Copahue volcano: Inversion of InSAR data using a genetic algorithm, *Journal of Volcanology and Geothermal Research* 202 (1-2) 117–126.

[6] Massonne, D. & Feigl, K. (1998). Radar Interferometry and its application to changes in the Earth's Surface, *Reviews of Geophysics* 36 (4) 441–500.

[7] Wright, E. M., Pardo Duró, M. L., Carballo, F. D. & Heredia, S. (2022). Detection of deformation at Socompa volcano from Differential Interferometry (DInSAR)XX Simposio Internacional SELPER, Monterrey, Nuevo León, México - October 26 to 28, 2022, available online at: https://www.selper.org.mx/wp-content/uploads/2023/03/Memorias-XX-SELPER-International-3.pdf.

[8] Liu Fei, Elliott, J. R., Ebmeier, S. K., Craig, T. J., Hooper, A., Novoa Lizama, C., and Delgado, F. (2022). First onset of unrest captured geodetically at Socompa Volcano, Northern Chile. Authorea. December 10, 2022, doi: 10.22541/essoar.167065592.28839515/v1.

[9] Guevara, L., & Giordanengo, G. (2023). Prospección Geofísica Magnetotelúrica Socompa 2021, Reporte Técnico, Serie Contribuciones Técnicas Geofísicas N° 18, Instituto de Geología y Recursos Minerales (IGRM), Servicio Geológico Minero Argentino (SEGEMAR), Dirección de Geomática, p. 12.

[10] Conde Serra, A. (2023). Condiciones de favorabilidad para la existencia de un sistema geotérmico activo en el área del Volcán Socompa, Departamento Los Andes, Provincia de Salta, Instituto de Geología y Recursos Minerales, Servicio Geológico Minero Argentino, Serie Contribuciones Técnicas Geotermia N° 6, Buenos Aires, p. 14.

[11] Seggiaro, R. E., & Apaza, F. (2018). Geología del Proyecto Geotérmico Socompa, Buenos Aires, Servicio Geológico Minero Argentino, Instituto de Geología y Recursos Minerales, p. 26.

[12] Zappettini, E. O., and Blasco, G. (2001). Hoja Geológica 2569-II, Socompa. Provincia de Salta. Instituto de Geología y Recursos Minerales, Servicio Geológico Minero Argentino, Boletín 260, Buenos Aires, p. 62.

[13] Conde Serra, A. (2017). Volcán Socompa. Exploración Geotérmica. Ministerio de Energía y Minería. Secretaría de Minería. Servicio Geológico Minero Argentino (SEGEMAR); Argentina, Buenos Aires, p. 20.

[14] Nevada Geodetic Laboratory DOI link for this station: https://doi.org/10.7283/T5TT4P27, Station operator information from: RINEX headers, available online at: http://geodesy.unr.edu/NGLStationPages/stations/SOCM.sta.

[15] Berardino, P., Fornaro, G., Lanari, R., & Sansosti, E. A. (2002). New Algorithm for Surface Deformation Monitoring Based on Small Baseline Differential SAR Interferograms, *IEEE Transactions on Geoscience and Remote Sensing 40* (11).

[16] Cao, Y., Jónsson, S., & Li, Z. (2021). Robust InSAR Tropospheric Delay Correction Using Global Atmospheric Models, EGU General Assembly 2021, online, 19–30 Apr. 2021, EGU21-11636, doi: https://doi.org/10.5194/egusphere-egu21-11636.

[17] Jolivet, R., Grandin, R., Lasserre, C., Doin, M. P., & Peltzer, G. (2011). Systematic InSAR tropospheric phase delay corrections from global meteorological reanalysis data, *Geophys. Res. Lett. 38*: L17311, doi: 10.1029/2011GL048757.